JOURNAL OF GUIDANCE, CONTROL, AND DYNAMICS
Vol. 26, No. 6, November–December 2003

Attitude Control of a Reentry Vehicle with Internal Dynamics

Elmar M. Wallner* and Klaus H. Well†
University of Stuttgart, 70550 Stuttgart, Germany

A control design for the X-38 reentry vehicle is presented. During a certain phase of reentry flight, attitude control has to be accomplished using only two control effectors. This limits the number of controlled variables for which decoupled tracking can be realized. It is shown that an inappropriate selection of the output gives rise to unacceptable internal dynamics when applying inversion-based control. Therefore, the zero dynamics are locally stabilized by means of an output-redefinition technique. An optimal pole placement enhances the robustness of the zero dynamics with regard to parametric model uncertainty. Further, a direct adaptive controller using a cerebellar model articulation controller neural network ensures tracking performance in the redefined outputs in the presence of model uncertainty. Simulation results are presented to confirm that stabilization of the zero dynamics, and adequate tracking performance are achieved. Because only a minimal set of control effectors is used, such a control scheme could represent a contribution toward a less costly return from space.

I. Introduction

FEEDBACK linearization (FBL) has attracted much interest in flight-control research over the past 10 years. A comprehensive treatment of the theory of FBL can be found in Ref. 1. When applied to flight-control problems, the underlying method is often referred to as dynamic inversion (DI).[2] Variants of DI control include robust dynamic inversion,[3] approximate feedback linearization,[4] and successive dynamic inversion based on timescale separation.[5] Additionally, concepts involving neural networks to augment inversion controllers in a direct adaptive control setting have been proposed.[6]

An important issue associated with the method is internal dynamics. The application of DI requires the stability of the associated zero dynamics, which can occur in the case of input/output linearization. In terms of linear system theory, unstable zero dynamics (or hidden modes) occur when DI is applied to a system with right-half plane transmission zeros (nonminimum phase systems). A tail-controlled skid-to-turn missile for example exhibits pronounced nonminimum phase behavior in its transfer function from fin deflection to normal acceleration as illustrated in Ref. 7. In some cases, nonminimum phase zero dynamics can be cured with approximate feedback linearization techniques as is commonly done in flight control. Here, FBL is applied to system dynamics, which are close to the true dynamics. The output-redefinition technique, as introduced in Ref. 8, offers another very effective approach and aims at stabilizing the zero dynamics while ensuring asymptotic tracking.

In this paper we deal with the attitude control problem of the X-38 reentry vehicle. As can be seen from Fig. 1, the X-38 utilizes different sets of actuators for control. These consist of either pure reaction control system, pure aerosurface control, or a mix of both. We are in particular concerned with the flight phase where only the two body flaps (elevons) are available for control. Actually, a significant portion of the reentry has to be accomplished with this minimal set of actuators. As will be shown, control of the bank angle via direct inversion leads to an unsatisfactory, nearly nonminimum phase behavior of the zero dynamics. This then motivates a modified approach to dynamic inversion, which is based on the output-redefinition technique. An enhancement of robustness of the zero dynamics with respect to parametric modeling errors is introduced by means of an optimal pole placement strategy. FBL is then applied to the system with the newly defined output. To ensure the linearization of the system's input/output behavior in the presence of unknown model dynamics, a neural-network-based, direct adaptive control scheme is brought to bear on the approximately feedback linearized dynamics.

This research adds to the field of control in general by providing a conclusive approach to integrating the notions of dynamic inversion and adaptive control in the presence of internal dynamics. In our view this control problem is also of general interest because it provides an illustrative example for the detrimental effects, which can be caused by internal dynamics and how to remedy such a defect. As for reentry flight control in particular, the approach we take is of interest because future return vehicle configurations are likely to bring about similar issues as those posed by X-38. Furthermore, most research results presented heretofore on flight control with internal dynamics have been restricted to the longitudinal motion (for example, see Refs. 7 and 9). Our work brings forward an example where pronounced internal dynamics occur in the lateral/directional motion.

The paper proceeds as follows: We will first recall the essentials of the feedback linearization method and subsequently demonstrate its application to the X-38 dynamics. This is followed by an elaboration on the output-redefinition approach and the optimal pole placement. Next, an outline of the underlying stability proof of the adaptive control scheme considering internal dynamics is presented. Nonlinear simulation results and a discussion conclude the paper.

II. Dynamic Inversion

Consider a system that is affine in the controls:

$$\dot{x} = f(x) + G(x)u, \qquad y = h(x)$$

where $u = [u_1 \ \cdots \ u_m]^T$, $y = [y_1 \ \cdots \ y_m]^T$, $G(x) = [g_1(x) \ \cdots \ g_m(x)]$, and $h(x) = [h_1(x) \ \cdots \ h_m(x)]^T$. The vector fields $f(x)$, $g_1(x), \ldots, g_m(x)$ are assumed to be smooth, and $h_1(x), \ldots, h_m(x)$ are smooth functions, all defined on $\mathbb{R}^n$. Supposing the system has a vector relative degree $[\rho_1, \ldots, \rho_m]$ at a point x_0 and that $\rho = \sum \rho_i < n$, there exists a local coordinate transformation $\phi(x): x \to (\xi, \eta)$ such that the preceding system is transformed into normal form.[1] The m dynamic equations of this normal form, which depend explicitly on the controls, can be put in the following compact representation:

$$\dot{\xi}_\rho = b(\xi, \eta) + A(\xi, \eta)u \tag{1}$$

Received 7 June 2002; presented as Paper 2002-4647 at the AIAA Guidance, Navigation, and Control Conference, Montreal, QC, Canada, 5–8 August 2002; revision received 31 January 2003; accepted for publication 9 June 2003.

*Ph.D. Candidate, Institute of Flight Mechanics and Control, Pfaffenwaldring 7a.

†Professor, Institute of Flight Mechanics and Control, Pfaffenwaldring 7a. Member AIAA.

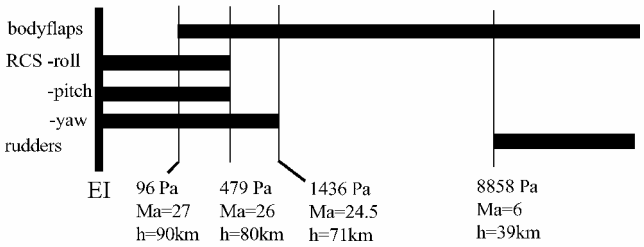

Fig. 1 Actuator schedule following entry interface. (Top numbers indicate dynamic pressure.)

with $\xi_\rho = [\xi_{\rho_1}^1 \ \cdots \ \xi_{\rho_m}^m]^T$. The exact linearization of the input/output relationship is achieved with the inversion law

$$u = A^{-1}(\xi, \eta)[-b(\xi, \eta) + \nu] \tag{2}$$

Insertion of Eq. (2) into the normal form yields

$$\dot{\xi}_j^i = \xi_{j+1}^i, \qquad j = 1 \cdots \rho_i - 1 \tag{3}$$

$$\dot{\xi}_{\rho_i}^i = \nu_i \tag{4}$$

$$\dot{\eta} = q(\xi, \eta) \tag{5}$$

$$y_i = \xi_1^i \tag{6}$$

with $1 \le i \le m$ and ν_i being the pseudocontrol of the ith control channel. Equation (5) represents the so-called internal dynamics. The design of any meaningful control law for the input/output linearized system depends fully on the behavior of the internal dynamics. Assume that for the external dynamics an asymptotic tracking control law has been designed. It can be shown (see Ref. 10) that, in the case of a local tracking control problem, local input-to-state stability (ISS) of the internal dynamics (where ξ is regarded as the input to the internal dynamics) is sufficient to locally guarantee bounded internal dynamics.

Sufficient conditions for local ISS of the internal dynamics can, in turn, be established via the notion of zero dynamics. These are defined as the dynamics of

$$\dot{\eta} = q(0, \eta) \tag{7}$$

Assume that the origin $\eta = 0$ is an equilibrium point of system (7). Asymptotic stability of this equilibrium point is then a sufficient condition for locally input-to-state stable internal dynamics.[10] In general, systems with asymptotically stable zero dynamics are called minimum phase systems.

III. Direct Inversion Applied to X-38

The equations governing the rigid-body attitude dynamics of the vehicle are given as follows. For control design and analysis we assume an affine system as given in Eq. (1) with $n = 6$ and state vector $x = [\alpha \ \beta \ \mu \ p \ \bar{q} \ \bar{r}]^T$. The symbols have the usual flight mechanical meanings, which are angle of attack, sideslip angle, bank angle, roll, pitch, and yaw rate, respectively. The nonstandard symbols $\bar{q}$ and $\bar{r}$ are used to avoid confusion with standard symbols from nonlinear control theory. The controls are elevator and aileron: $u = [\Delta\delta_e \ \ \delta_a]^T$. The drift term $f(x) = [f_1(x) \ \cdots \ f_n(x)]^T$ is composed of the following elements:

$$f_1(x) = \bar{q} - \tan\beta(p\cos\alpha + \bar{r}\sin\alpha) - \frac{1}{mV_f\cos\beta}(L - mg_0\cos\gamma_f\cos\mu)$$

$$f_2(x) = p\sin\alpha - \bar{r}\cos\alpha + \frac{1}{mV_f}(-Y_\beta\beta + mg_0\cos\gamma_f\sin\mu)$$

$$f_3(x) = \frac{1}{\cos\beta}(p\cos\alpha + \bar{r}\sin\alpha) + \frac{\tan\beta}{mV_f}(L - mg_0\cos\gamma_f\cos\mu) + \frac{\tan\gamma_f}{mV_f}(L\sin\mu - Y_\beta\beta\cos\mu)$$

$$f_4(x) = L'_\beta\beta + \frac{\{p\bar{q}I_{xz}(I_{zz} + I_{xx} - I_{yy}) + \bar{q}\bar{r}[I_{zz}(I_{yy} - I_{zz}) - I_{xz}^2]\}}{(I_{xx}I_{zz} - I_{xz}^2)}$$

$$f_5(x) = M'_\alpha\Delta\alpha + \frac{[(I_{zz} - I_{xx})p\bar{r} + I_{xz}(\bar{r}^2 - p^2)]}{I_{yy}}$$

$$f_6(x) = N'_\beta\beta + \frac{\{p\bar{q}[I_{xz}^2 + I_{xx}(I_{xx} - I_{yy})] + \bar{q}\bar{r}I_{xz}(I_{yy} - I_{xx} - I_{zz})\}}{(I_{xx}I_{zz} - I_{xz}^2)} \tag{8}$$

We let $\Delta\alpha = \alpha - \alpha_T$ and $\Delta\delta_e = \delta_e - \delta_{eT}$ denote deviations from trim condition. The trim angle of attack α_T is usually a prescribed function of Mach number. Because Mach number evolves much slower than the attitude dynamics, α_T is taken as constant for the purpose of stability analysis. The trim elevator deflection δ_{eT} corresponds to the elevator setting for which the vehicle is free of pitch moment at trim angle-of-attack conditions. The control distribution matrix is taken to have the form

$$G = \begin{bmatrix} 0 & L'_{\delta a} \\ M'_{\delta e} & 0 \\ 0 & N'_{\delta a} \end{bmatrix} \tag{9}$$

In the preceding, m, g_0, γ_f, V_f, L, Y denote vehicle mass, gravitational acceleration, flight-path angle, flight-path speed, lift and side forces, respectively. We take γ_f, V_f, and g_0 as constant because these variables evolve much slower than the attitude and angular rate states. We arrive at the affine representation of the system by linearly approximating the dependency of the aerodynamic moments on the states and controls about the trim condition. This is justifiable because all our subsequent analyses will be local and a control law will be applied, which accounts specifically for model errors ensuing from such a linear approximation. Note that we have neglected the damping derivatives. This is generally a viable assumption for a lifting body in the hypersonic flight regime. The effect of the control effectors on side and lift force will be neglected likewise, that is, all derivatives of the type Y_δ and L_δ are taken as zero. This is a common assumption based on the concept of the approximate FBL technique,[4] and the fact that, in general, aircraft control surfaces are primarily moment-producing devices. This approach has proven practicable in many flight-control applications (for example, see Ref. 5), and it facilitiates the design process. The simulation results to be presented in this paper confirm that this also holds true in the case of X-38. Force effects of the flaps are however included in the simulation model. The inversion can therefore be exact only with respect to the simplified model dynamics while being approximate with regard to the true dynamics. The linear approximation of the system about its equilibrium is state controllable.

Because only two controls are available ($m = 2$), we can achieve decoupled tracking control of only two outputs. In a first step we take the system output as

$$y = [\Delta\alpha \quad \mu]^T \tag{10}$$

At first glance this choice seems reasonable as α and μ are the key variables to influence the reentry trajectory and are commanded by guidance algorithms. Because of the neglect of the force contributions of the controls, the system possesses a vector relative degree [2 2]. Because $\rho = 4$ is less than the number of states, dynamic inversion will inevitably lead to internal dynamics. The transition to normal form is attained with a state transformation $[\xi^T \ \ \eta^T]^T = \Phi(x)$, which is determined by

$$\xi = \begin{bmatrix} \Delta\alpha \\ f_1(x) \\ \mu \\ f_3(x) \end{bmatrix}, \qquad \eta = \begin{bmatrix} \beta \\ \dfrac{p}{L'_{\delta a}} - \dfrac{\bar{r}}{N'_{\delta a}} \end{bmatrix} \tag{11}$$

where $\xi = [\xi_1^1 \ \ \xi_2^1 \ \ \xi_1^2 \ \ \xi_2^2]^T$ and $\eta = [\eta_1 \ \ \eta_2]^T$. This transformation yields a normal form with internal dynamics as in Eq. (5). The

stability of the zero dynamics is analyzed locally at the equilibrium, that is, by checking the system poles of the linearized internal dynamics. Note that the origin $(\xi, \eta) = (0, 0)$ is an equilibrium point of the unforced (i.e., $\delta_a = \Delta\delta_e = 0$) dynamics in normal form. The poles are depicted in Fig. 2 for a nominal reentry according to NASA's Cycle 8 reference trajectory.[11] As can be seen, the poles are very lightly damped and even unstable at lower altitudes. Two numerical examples of the design state matrices and zeros are given in the Appendix. (The examples include the model simplifications just discussed.) From these zero dynamics we would expect unsatisfactory behavior of the internal dynamics. This is confirmed by nonlinear simulation results as depicted in Fig. 3. Simulation details will be given in a subsequent section. An inversion-based tracking control law [using proportional–integral–derivative (PID) compensators] is designed so that the output tracks a desired bounded and smooth output:

$$y_d = [\Delta\alpha_d(t) \quad \mu_d(t)]^T \tag{12}$$

As can be seen, the bank angle tracking is fairly satisfactory. However, the maneuver excites the internal system dynamics, which results in a nearly undamped, though bounded, oscillation in sideslip angle. Obviously, this is unacceptable as these oscillations would entail energy-consuming actuator activity, detrimental side heating of the vehicle, degraded flight performance, and passenger discomfort. Therefore, remedial measures had to be taken to adequately stabilize the zero dynamics. This is detailed in the following section.

IV. Stabilization of Zero Dynamics

A detailed account of the output-redefinition method from Gopalswamy and Hedrick is given in Ref. 8. In our work we apply output-redefinition in a similar manner to the X-38 control problem. The redefinition proceeds in three steps. In the first step the internal dynamics pertaining to the original output y are identified. This has already been illustrated in the preceding section. As shown, we cannot directly impose a desired transient behavior on the bank angle (because of unacceptable internal stability). Consequently, we choose to indirectly achieve tracking performance. To this end, in the second step the relative degree is reduced to one in the lateral control channel so that the bank angle μ becomes a state variable of the resulting internal dynamics. In the third step the output is redefined in such a way that the zero dynamics are (locally) stabilized. A correspondingly redefined reference input in the lateral channel ensures that adequate tracking performance in bank angle is retained.

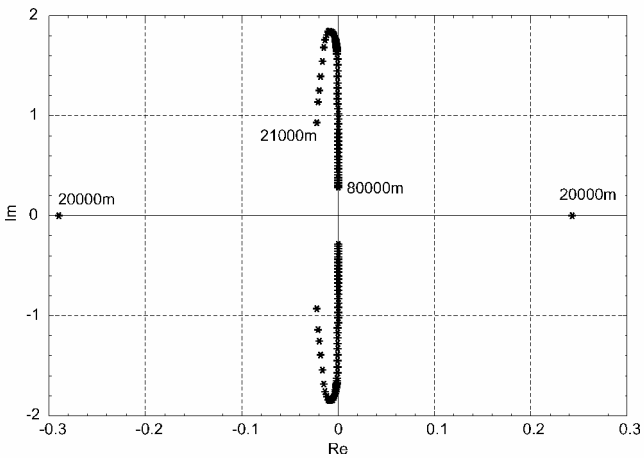

Fig. 2 Poles of unmodified zero dynamics for Cycle 8 reentry trajectory. (Numbers indicate flight altitude.)

In terms of the normal form coordinates, the original output reads

$$y = \begin{bmatrix} \xi_1^1 & \xi_1^2 \end{bmatrix}^T$$

The system relative degree is now reduced by means of the following modifed output selection:

$$S = \begin{bmatrix} \Delta\alpha \\ \dot{\mu} + \kappa\mu \end{bmatrix} = \begin{bmatrix} \xi_1^1 \\ \xi_2^2 + \kappa\xi_1^2 \end{bmatrix} \tag{13}$$

with design parameter $\kappa > 0$. (We select $\kappa = 1$.) Note that now the relative degree is [2 1]. The corresponding desired output is denoted by

$$S_d(t) = \begin{bmatrix} \Delta\alpha_d(t) \\ \dot{\mu}_d(t) + \kappa\mu_d(t) \end{bmatrix} \tag{14}$$

Based on this output, a secondary state transformation is defined:

$$\begin{bmatrix} \xi_1^{1*} \\ \xi_2^{1*} \\ \xi_1^{2*} \end{bmatrix} = \begin{bmatrix} \xi_1^1 \\ \xi_2^1 \\ \xi_2^2 + \kappa\xi_1^2 \end{bmatrix}, \qquad \begin{bmatrix} \eta_1^* \\ \eta_2^* \\ \eta_3^* \end{bmatrix} = \begin{bmatrix} \xi_1^2 \\ \eta_1 \\ \eta_2 \end{bmatrix} \tag{15}$$

Note that the bank angle η_1^* is now an internal state variable. With this transformation the system can be represented in the new normal form. In particular, the corresponding internal dynamics can be expanded as

$$\dot{\eta}^* = P\xi^* + Q\eta^* + a_1(\xi^*, \eta^*) \tag{16}$$

where $a_1(\xi^*, \eta^*)$ contains terms of higher order. In the case that the output tracks the desired output perfectly, that is, $S(t) = S_d(t)$, the internal dynamics take the form

$$\dot{\eta}_d^* = P\xi_d^* + Q\eta_d^* + a_1\left(\xi_d^*, \eta_d^*\right) \tag{17}$$

where

$$\xi_d^*(t) = [S_{1d}(t) \quad \dot{S}_{1d}(t) \quad S_{2d}(t)]^T \tag{18}$$

is the desired external state corresponding to the desired output behavior $S_d(t)$. If there exists an acceptable solution $\eta_d^*(t)$ or, equivalently, an initial state such that $\eta_d^*(t)$ is bounded and deemed acceptable, then we call $\eta_d^*(t)$ the ideal internal dynamics (IID).

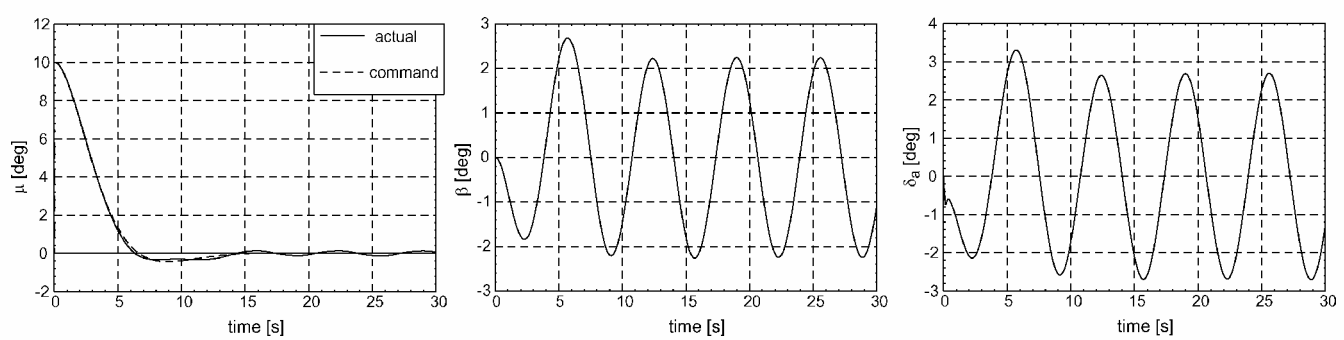

Fig. 3 Step responses of unmodified output for initial altitude $h(0) = 60$ km ($Ma = 18.5$).

In the preceding we have modified the original output y to obtain the output $S = [\xi_1^{1*} \;\; \xi_1^{2*}]^T$. We now proceed with the actual redefinition of the output S, which is as follows:

$$\bar{S} = S - K\eta^*, \qquad K = \begin{bmatrix} 0_{1\times 3} \\ k^T \end{bmatrix} \tag{19}$$

and $k = [k_1 \;\; k_2 \;\; k_3]^T$. The desired redefined output is taken as

$$\bar{S}_d(t) = S_d(t) - K\eta_d^*(t) \tag{20}$$

where S_d and η_d^* have been defined earlier. The dynamics in normal form corresponding to the redefined output can be easily deduced from the following state transformation:

$$\begin{bmatrix} \bar{\xi}_1^1 \\ \bar{\xi}_2^1 \\ \bar{\xi}_1^2 \end{bmatrix} = \begin{bmatrix} \xi_1^{1*} \\ \xi_2^{1*} \\ \xi_1^{2*} - k^T\eta^* \end{bmatrix}, \qquad \begin{bmatrix} \bar{\eta}_1 \\ \bar{\eta}_2 \\ \bar{\eta}_3 \end{bmatrix} = \begin{bmatrix} \eta_1^* \\ \eta_2^* \\ \eta_3^* \end{bmatrix} \tag{21}$$

According to the state transformation (21), the desired output in Eq. (20) is equivalent to the following desired states:

$$\bar{\xi}_d(t) = \xi_d^*(t) - K'\eta_d^*(t), \qquad K' = \begin{bmatrix} 0_{1\times 3} \\ K \end{bmatrix} \tag{22}$$

Consider for a moment the idealized case of perfect tracking control so that after finite time $T > 0$ perfect tracking in the modified output is achieved, that is, $\bar{S}(t) \equiv \bar{S}_d(t)$ or, equivalently, $\bar{\xi}(t) \equiv \bar{\xi}_d(t)$ for all $t \geq T$. In this case,[8] we can write the dynamics of the error variable $\tilde{\eta} = \bar{\eta} - \eta_d^*$ as

$$\dot{\tilde{\eta}} = [PK' + Q]\tilde{\eta} + a_2(\bar{\xi}_d, \eta_d^*, \tilde{\eta}) \tag{23}$$

From this development we can now infer two things. First of all, selecting K to the effect that the eigenvalues of $[PK' + Q]$ have negative real part ensures locally asymptotically stable zero dynamics.[8] This, in turn, is sufficient for guaranteeing local ISS of the internal dynamics. Note that arbitrary pole placement is possible because of the system's state controllability.[8] Second, Eq. (23) clarifies how asymptotic tracking is attained. With the adaptive tracking control law to be presented subsequently, not perfect tracking but, at most, asymptotic tracking can be attained so that we have $\bar{S}(t) \to \bar{S}_d(t)$ asymptotically. In this case the actual dynamics of the error variable $\tilde{\eta}$ approach the ideal dynamics (23) asymptotically. Thereby, the internal dynamics approach the IID asymptotically so that $\tilde{\eta} \to 0$. Given Eqs. (19) and (20), this in turn leads to $S(t) \to S_d(t)$ so that eventually, because of the definitions in Eqs. (13) and (14), we have $y(t) \to y_d(t)$.

A central point is the formulation of the IID because this directly affects the achievable tracking performance in the original outputs. Asymptotic tracking as just described can only be achieved if $\eta_d^*(t)$ solves Eq. (17) for some bounded $\xi_d^*(t)$. Because obtaining a general solution to this problem can become rather involved,[8] we have chosen to solve Eq. (17) only for the special case of a step input in bank angle, that is, $\mu_d(t) = \mu_c$ with μ_c taken as constant. The corresponding desired state is then $\xi_d^* = [0 \;\; 0 \;\; \kappa\mu_c]^T$. The steady-state solution is one possible solution that we have adopted as the IID. This selection prevents steady-state tracking errors. Although we consider only a special case of IID, simulation results have shown that adequate transient tracking behavior is achieved when the desired bank angle $\mu_d(t)$ actually varies with time. We also found that the performance of guidance algorithms is not compromised by this procedure.

V. Selection of Zero Dynamics

A main issue of output redefinition lies in the selection of the modified output, which is determined by the entries of K. As mentioned, we can place the system poles of the zero dynamics by varying the output parameters k_1, k_2, k_3. Kim and Tahk have proposed an approach in Ref. 7 that aims at placing the poles so that the sensitivity of the pole locations with respect to parametric modeling errors is minimized. We have adopted the basic notion of this approach for our application. Recall that the coordinate transformation (11) invoked earlier to obtain a normal form representation involved model parameters. These parameters are actually uncertain. Hence, as an extension to the development made thus far we need to account for the impact of modeling errors on the state transformation. Consider again the redefined output (19), which, according to the preceding development, can be written in original coordinates as

$$y_1 = \Delta\alpha$$

$$y_2 = \dot{\mu} + (\kappa - k_1)\mu - k_2\beta - k_3\left(\bar{p}\big/\hat{L}'_{\delta_a} - \bar{r}\big/\hat{N}'_{\delta_a}\right) \tag{24}$$

The redefined output is henceforth denoted by y. For this output we define a transformation that leads to a normal form representation of the system dynamics in the presence of model uncertainty:

$$\xi_1^1 = \Delta\alpha, \qquad \xi_2^1 = f_1(x)$$

$$\xi_1^2 = f_3(x) + (\kappa - k_1)\mu - k_2\beta - k_3\left(\bar{p}\big/\hat{L}'_{\delta_a} - \bar{r}\big/\hat{N}'_{\delta_a}\right)$$

$$\eta_1 = \mu, \qquad \eta_2 = \beta, \qquad \eta_3 = \bar{p}\big/L'_{\delta_a} - \bar{r}\big/N'_{\delta_a} \tag{25}$$

We henceforth let ξ and η denote the transformed state variables. Essentially, this transformation represents a generalization of the coordinate transformation we have applied in the preceding sections. Note that the transformation (25) distinguishes between the assumed (nominal) model parameters $\hat{L}'_{\delta_a}$, $\hat{N}'_{\delta_a}$ and the actual unknown parameters L'_{δ_a}, N'_{δ_a}. In the nominal case, as treated in the preceding section, these are identical. We assume that the relations in Eq. (25) represent a local state transformation in a neighborhood of the equilibrium point for the nonnominal case as well. Closer examination has shown this to be a valid assumption for expected parameter variations.

With the preceding transformation we obtain the dynamics in a normal form representation. The associated internal dynamics are linearized about the equilibrium, which is the origin of the state space. The linearized internal dynamics take the general form

$$\dot{\eta} = P_\Delta\xi + [P_\Delta K' + Q_\Delta]\eta \tag{26}$$

We introduce the notations P_Δ, Q_Δ to distinguish the uncertain system matrices from their nominal counterparts P, Q from the preceding section.

We arrive at a pole placement strategy as follows: Let the system poles of the zero dynamics associated with the preceding linearized internal dynamics be denoted by λ_k. Further, the right and left eigenvectors of the corresponding eigenvalue problem are represented by v_k and w_k, respectively. Now let $\theta = [\theta_1 \;\; \cdots \;\; \theta_{n_p}]^T$ represent the model parameters with regard to which we seek to reduce the sensitivity of the zero dynamics. Here, n_p denotes the number of uncertain parameters considered. The respective nominal parameter values, on the basis of which we have devised the coordinate transformation in the preceding section, are denoted by $\hat{\theta} = [\hat{\theta}_1 \;\; \cdots \;\; \hat{\theta}_{n_p}]^T$. According to Ref. 7, the sensitivity of the nominal pole locations can be assessed via the following relation:

$$\frac{\partial\lambda_k}{\partial\theta_j} = \hat{w}_k{}^T\frac{\partial[P_\Delta K' + Q_\Delta]}{\partial\theta_j}\hat{v}_k \tag{27}$$

for $k = 1, 2, 3$. In the preceding, $\hat{\lambda}_k$, $\hat{w}_k$, and $\hat{v}_k$ stand for the nominal eigenvalues and eigenvectors pertaining to the nominal system matrices P and Q. The derivatives are to be understood as taken for the nominal parameter values, that is, $\theta = \hat{\theta}$. Equation (27) can be used to formulate a measure J for the sensitivity of the nominal pole locations:

$$J = \sum_{k=1}^{n-\rho}\sum_{j=1}^{n_p}\frac{\partial\lambda_k}{\partial\theta_j}\left(\frac{\partial\lambda_k}{\partial\theta_j}\right)^* \tag{28}$$

Table 1 Constraints for nominal pole locations of zero dynamics

Criterion	$h \leq 60$ km	60 km $< h \leq 70$ km	$h > 70$ km
Minimum damping	0.6	0.6	0.6
Maximum time constant, s	1.11	1.43	2

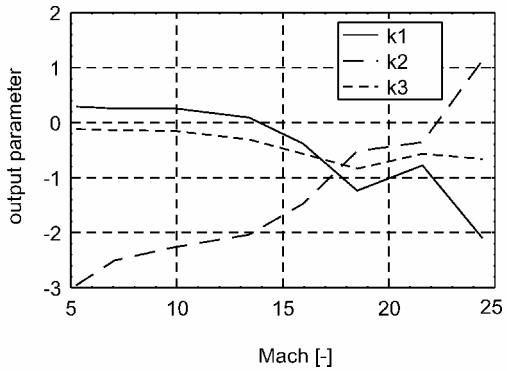

Fig. 4 Output parameter schedule for shaping of redefined output.

For our particular problem we have chosen $n_p = 4$. The uncertain parameters we consider are L'_{δ_a}, N'_{δ_a}, L'_β, N'_β. Using a standard sequential quadratic programming algorithm, we minimize the sensitivity of the nominal zero dynamics:

$$\min_{K'} J(K')$$

This optimization is conducted for several flight conditions along the nominal Cycle 8 trajectory so that, eventually, we obtain a controller encompassing a scheduling of the controlled variables. We have scheduled the parameters k_1, k_2, k_3 as a function of Mach number. Certainly, the scheduling dependency could be extended to include additional slowly varying scheduling variables such as dynamic pressure. Because the pole locations in the complex plane determine the achievable tracking performance, we have extended the preceding cost functional to allow for a constrained optimization. The constraints pertain to the nominal pole locations in the complex plane. They are chosen such that the nominal poles are confined to a prescribed area, which is determined by maximum allowed time constant and minimum allowed damping ratio of the poles as listed in Table 1. The selection of the boundaries of this area is based on simulation results obtained for step inputs in the controlled variables. (Simulation results are presented in a subsequent section.) Interestingly, for most Mach numbers the poles are placed close to the corners of the prescribed area corresponding to the maximum allowed time constant and minimum allowed damping. Hence, these conditions imply minimal sensitivity of the nominal pole locations to model uncertainty. It has been found that demanding overly small maximum time constants for very high-altitude flight conditions entails a comparably large sensitivity measure J, which impairs robustness of the closed-loop system. Consequently, the maximum time constant constraint is relaxed for higher flight altitudes h. The outcome of this design procedure, that is, the schedule of the parameters k_1, k_2, k_3, is depicted in Fig. 4. Numerical examples for two selected flight conditions are given in the Appendix.

VI. Direct Adaptive Control

Having now defined the controlled variables, we proceed with the design of an input/output linearizing controller. A direct adaptive control scheme is applied to ensure that feedback linearization is achieved in the presence of modeling errors. It comprises a cerebellar model articulation controller (CMAC) neural network to compensate for any inversion errors by adapting the controller so that the desired response of the controlled variables is recovered. The CMAC consists of receptive fields that are distributed overlappingly in the neural net input space.[12] Each receptive field

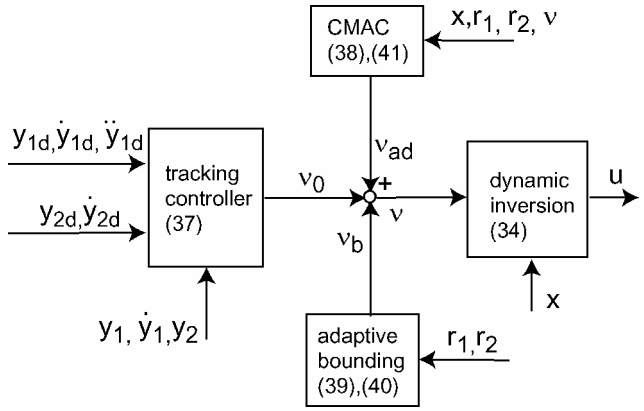

Fig. 5 Structure of adaptive inversion controller.

is associated with activation functions in a similar way as in radial basis function networks. Because each activation function has a compact support, only a subset of all receptive fields is excited by an input to the neural net.[12] A block diagram of the controller is given in Fig. 5. The numbers of the equations pertaining to the individual blocks are included in the diagram.

Let the desired outputs be bounded according to

$$\left\| [y_{1d}(t) \quad \dot{y}_{1d}(t) \quad \ddot{y}_{1d}(t) \quad y_{2d}(t) \quad \dot{y}_{2d}(t)]^T \right\| \leq b_{yd} \tag{29}$$

for some bounded $b_{yd} > 0$. For the modified output as given in Eq. (24), we define the associated tracking errors

$$e_1 = y_1 - y_{1d} \tag{30}$$

$$e_2 = y_2 - y_{2d} \tag{31}$$

and the filtered tracking errors

$$r_1 = \dot{e}_1 + \vartheta e_1 \tag{32}$$

$$r_2 = e_2 \tag{33}$$

with design parameter $\vartheta > 0$. The external states of the normal form are driven by dynamics as formulated in Eq. (1), whereby we arrive at the standard inversion law

$$u = \hat{A}(\xi, \eta)^{-1}[\nu - \hat{b}(\xi, \eta)] \tag{34}$$

This way we achieve an approximate inversion of the actual plant dynamics at most because the preceding inversion law is founded on the nominal dynamics determined by the nominal vector function $\hat{b}(\xi, \eta)$ and decoupling matrix $\hat{A}(\xi, \eta)$. The external dynamics of the true normal form, however, are governed by an equation of the form

$$\dot{\xi}_\rho = \hat{b}(\xi, \eta) + \hat{A}(\xi, \eta)u + \Delta(\xi, \eta, u) \tag{35}$$

where $\Delta(\xi, \eta, u)$ is a nonlinear vector function representing modeling errors. Note that the modeling error exhibits a dependency on the controls u. Because of this dependency, direct adaptive control laws ensuing from the widely accepted Lyapunov stability proofs suffer from an inherent fixed-point problem.[6] We are currently investigating a stability proof to circumvent the problem that will be reported elsewhere. For now we resolve the issue by solving the fixed-point problem within the control algorithm as proposed in Ref. 6. The pseudocontrol is chosen as

$$\nu = \nu_0 + \nu_b + \nu_{\text{ad}} \tag{36}$$

in which the nominal pseudocontrol ν_0 is selected as

$$\nu_0 = \begin{bmatrix} \ddot{y}_{1d} - k_1^c r_1 - \vartheta \dot{e}_1 \\ \dot{y}_{2d} - k_2^c r_2 \end{bmatrix} \tag{37}$$

with controller parameters k_1^c, $k_2^c > 0$. The nominal pseudocontrol is augmented by ν_{ad} and ν_b, which represent the neural network output and an adaptive bounding term, respectively. Now define $z = [\xi \;\; \eta]^T$. The CMAC is a linear-in-the-parameters network[12]; its output is given by

$$\nu_{ad} = -\hat{W}^T \Gamma(z, \nu) \tag{38}$$

where Γ stands for a vector of activation functions and $\hat{W}$ is a matrix containing the adaptable weights. This equation presents the just-mentioned fixed-point problem in the variable ν_{ad}. Note that the transformation to normal form (25) requires knowledge of actual model parameters. Because these are of course unknown, we are deprived of knowing the complete state vector z. Therefore, when implemented, the neural net recall equation (38) is driven by the state in original coordinates x rather than z. The adaptive bounding is introduced to compensate for network approximation errors similarly to Ref. 13:

$$\nu_{b_i} = \psi_i \tanh(r_i/\delta), \qquad i = 1, 2 \tag{39}$$

with design parameter $\delta > 0$. The adaptive terms serve to cancel the uncertain term Δ in the dynamic equations, thereby ensuring boundedness of the filtered error r. The adaptation laws are derived from Lyapunov stability theory, guaranteeing the ultimate boundedness of the tracking error $r = [r_1 \;\; r_2]^T$ and the boundedness of the network weights $\hat{W}$ as well as adaptive bounding parameters ψ. Note that boundedness of the filtered error implies boundedness of the actual tracking error e. The parameter tuning laws are

$$\dot{\psi}_i = \gamma[r_i \tanh(r_i/\delta) - \sigma_\psi \|r\| \psi_i] \tag{40}$$

$$\dot{\hat{W}} = \phi\left(\Gamma r^T - \sigma_W \|r\| M_\Gamma \hat{W}\right) \tag{41}$$

where γ and ϕ denote adaptation rates and the terms associated with σ_ψ, $\sigma_W > 0$ prevent parameter drift. The diagonal matrix M_Γ has entries that take the values of either 1 or 0, depending on whether the associated receptive field of the CMAC is being excited. A receptive field is regarded as being excited when the neural net input point lies inside the compact support of the corresponding activation function. Note further that only entries of Γ belonging to an excited receptive field can take nonzero values. The jth entry of Γ and the jth diagonal element of M_Γ pertain to the same receptive field. As a result, when a receptive field is not excited the weight update law (41) yields zero for the corresponding time derivative $\dot{\hat{W}}_{ji}$. That way, we ensure that only weights corresponding to excited receptors are updated at any instant.[12] For the sake of conciseness, we omit the derivation of these update laws and refer to Refs. 12 and 14 for details. The essence of the stability proof is that the filtered tracking error can be proven to be bounded, provided that the state of the system z remains inside a compact set $\Omega \subset \mathbb{R}^n$, where an assumed approximation capability of the neural network holds. We take the set Ω to contain the origin. The bound on the filtered tracking error can then be written as

$$\|r\| \le b_r = \|r(0)\| + \varepsilon_r \tag{42}$$

where $\varepsilon_r > 0$ can be made arbitrarily small by choice of controller parameters. (This is attained foremost by increasing the adaptation rates and the controller gains.) We further need to ensure the boundedness of the internal dynamics. Toward this, we impose the following assumptions regarding the zero dynamics.

Assumption: Consider the zero dynamics pertaining to the internal dynamics (5). The equilibrium point $(\xi, \eta) = (0, 0)$ is exponentially stable for all $(0, \eta) \in \Omega$. The function $q(\xi, \eta)$ is uniformly Lipschitz in ξ so that

$$\|q(\xi, \eta) - q(0, \eta)\| \le L_\xi \|\xi\|, \qquad \forall z \in \Omega \tag{43}$$

with Lipschitz constant $L_\xi > 0$.

This assumption is based on the fact that the output redefinition guarantees at least local exponential stability of the nonlinear zero dynamics under nominal conditions, whereas the robust pole placement aims at preserving this stability property under perturbed conditions. Because the zero dynamics are taken to be exponentially stable, there exists, according to a converse Lyapunov theorem (for example, see Ref. 10), a Lyapunov function $V_0(\eta)$, so that the following holds:

$$c_2\|\eta\|^2 \le V_0 \le c_1\|\eta\|^2 \tag{44}$$

$$\frac{\partial V_0}{\partial \eta} q(0, \eta) \le -c_3\|\eta\|^2 \tag{45}$$

$$\left\| \frac{\partial V_0}{\partial \eta} \right\| \le c_4\|\eta\| \tag{46}$$

with positive constants c_1, c_2, c_3, and c_4. As implicated by our recapitulation of FBL theory, local exponential stability of the zero dynamics is a sufficient condition for guaranteeing the local input-to-state stability of the internal dynamics. Because of the boundedness of the filtered tracking error and its definition in Eqs. (32) and (33), the state ξ is bounded as follows:

$$\begin{aligned} \|\xi\| &\le d_1\|e_1(0)\| + d_2\|r\| + b_{y_d} \\ &\le b_\xi = d_1\|e_1(0)\| + d_2 b_r + b_{y_d} \end{aligned} \tag{47}$$

for positive constants d_1 and d_2. The derivative of V_0 along the trajectories of the internal dynamics takes the form

$$\dot{V}_0(\eta) = \frac{\partial V_0}{\partial \eta} q(0, \eta) + \frac{\partial V_0}{\partial \eta}[q(\xi, \eta) - q(0, \eta)] \tag{48}$$

By applying the Lipschitz condition, the converse Lyapunov theorem and Eq. (47), we can infer

$$\begin{aligned} \dot{V}_0(\eta) &\le -c_3\|\eta\|^2 + c_4\|\eta\| L_\xi \|\xi\| \\ &\le -c_3\|\eta\|^2 + c_4\|\eta\| L_\xi \left[d_1\|e_1(0)\| + d_2\|r\| + b_{y_d}\right] \end{aligned} \tag{49}$$

Thus, we can state that $\dot{V}_0(\eta) < 0$ whenever

$$\|\eta\| > k_\eta = (c_4/c_3) L_\xi \left[d_1\|e_1(0)\| + d_2 b_r + b_{y_d}\right] \tag{50}$$

This implies that the internal dynamics are bounded as long as $\|r\|$ is bounded. This, in turn, is ensured by the direct adaptive controller, provided that $z \in \Omega$. Hence, the boundedness of the internal dynamics can be put as follows:

$$\|\eta\| \le b_\eta = \max\{\|\eta(0)\|, \quad k_\eta + \varepsilon_\eta\} \tag{51}$$

for some arbitrarily small $\varepsilon_\eta > 0$. For completion of the stability proof, it can then be shown that if the initial state satisfies $z(0) \in \Omega$ then it can be ensured that the state does not escape from the set Ω (for details see Ref. 14). This is because, according to Eq. (42), the filtered tracking error bound b_r in Eq. (42) can be reduced by choice of controller parameters to the extent that it approaches the initial tracking error norm $\|r(0)\|$. Further, the tracking command bound b_{y_d} can be reduced so as to keep the state inside the set Ω.

VII. Simulation

To demonstrate the effectiveness of the proposed controller, we now present nonlinear simulation results. The aerodynamics and other parameters of the vehicle are formulated in accordance with the simulation model developed within the German TETRA research program on reentry technologies. These issues are discussed in Ref. 15. For simulation in six degrees of freedom, the equations of motion for a rigid-body vehicle have been formulated for flight over a spherical rotating Earth.[15] A fourth-order Runge–Kutta scheme is used to numerically integrate the equations of motion. The atmospheric data correspond to that of the Cycle 8 trajectory.[11]

Second-order actuator models with a damping ratio of 0.7 and natural frequency of 26 rad/s are included as well. Note that the aerodynamic model includes the features that have been neglected for control design purposes, that is, aerodynamic damping moments caused by angular rates as well as the aerodynamic force effects of the control surfaces are considered in the simulation model. The controller parameters are selected as follows: $\vartheta = 1.0$, $k_1^c = 2.0$, and $k_2^c = 2.0$. These parameters were found to yield adequate tracking performance for nominal conditions. As for the adaptation laws, the following parameters are chosen: $\delta = 0.1$, $\gamma = 20$, $\phi = 1$, $\sigma_\psi = 0.01$, and $\sigma_W = 0.01$. Separate CMAC networks are implemented in the longitudinal and lateral control channels as is commonly done by other researchers.[6] In the longitudinal channel net 16 CMAC receptors are excited at every instant so that the same number of weights need to be updated at every time step. In the lateral channel this number is increased to 32.

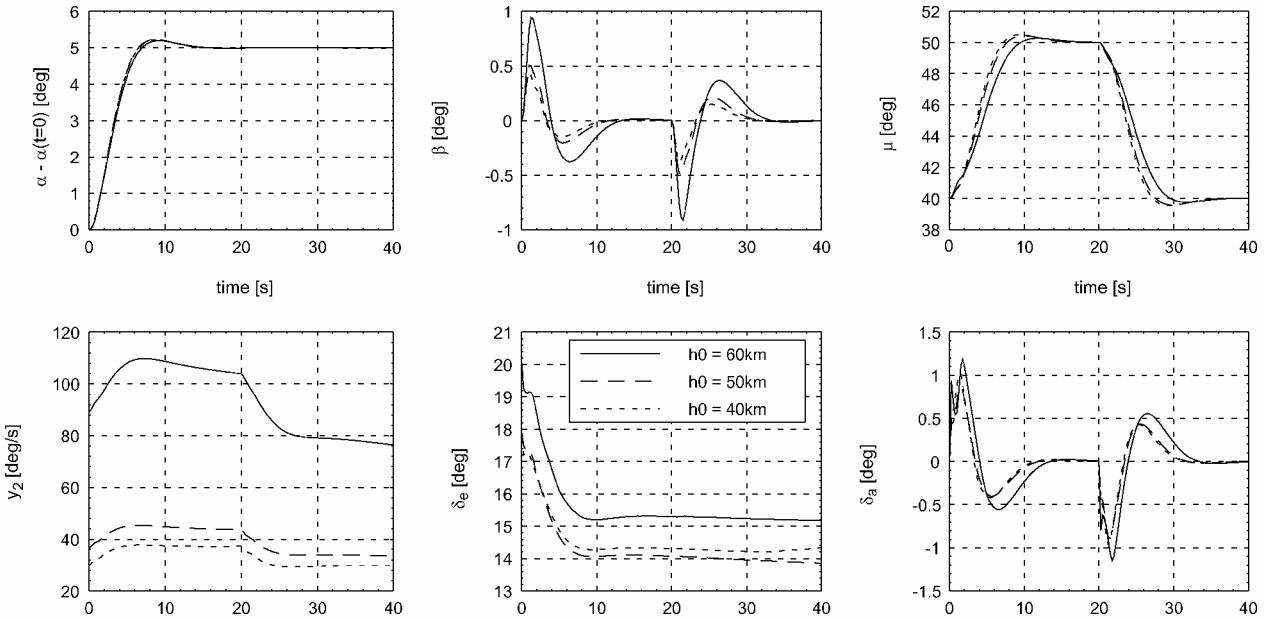

Fig. 6 Step responses for redefined output at different altitudes [$h(0) = 60$ km/$Ma = 18.5$, $h(0) = 50$ km/$Ma = 13.4$, $h(0) = 40$ km/$Ma = 7$].

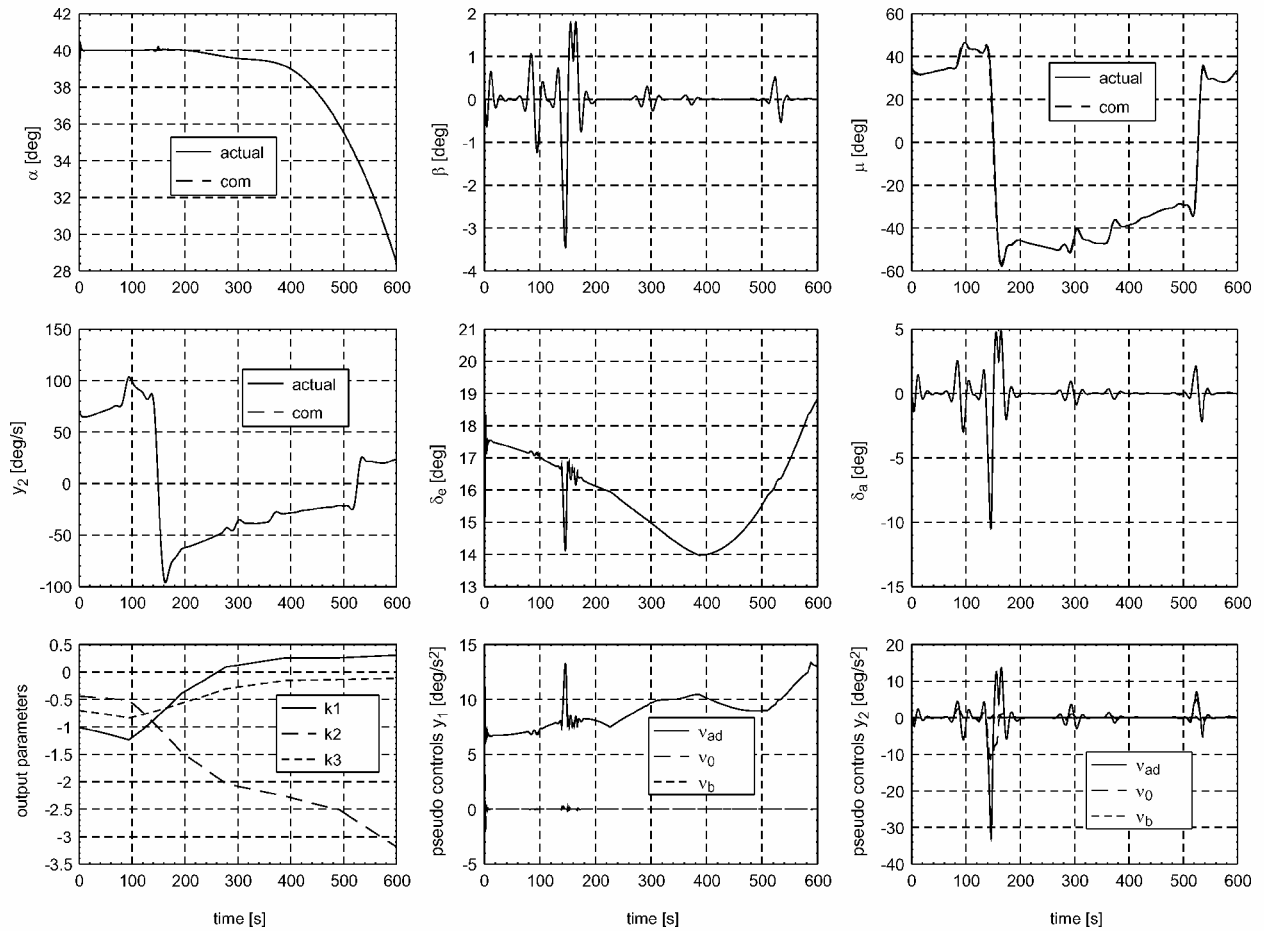

Fig. 7 Tracking of Cycle 8 attitude commands.

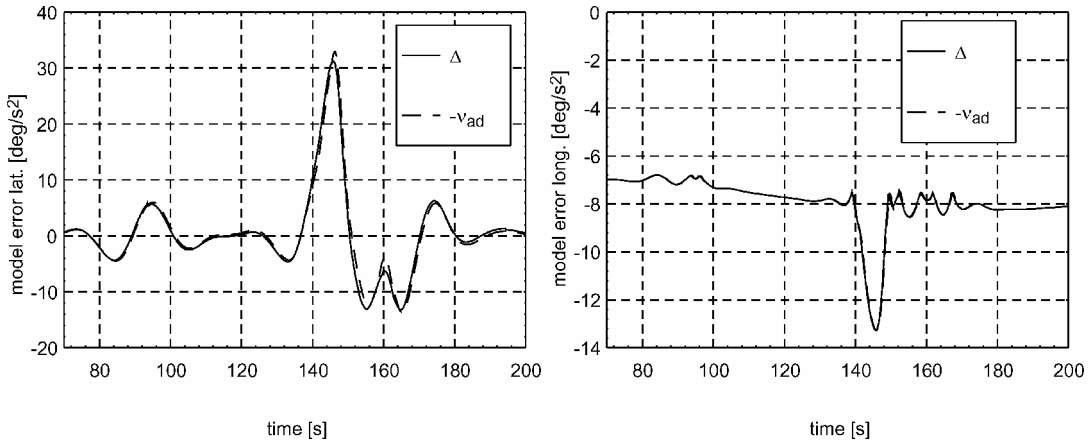

Fig. 8 Model errors and neural-network approximation.

Figure 6 shows the response to step inputs in angle of attack (5-deg step relative to initial α) and bank angle (10-deg step relative to initial μ) commands at different altitudes. The controller accomplishes to track the α as well as the modified output y_2 commands. This leads to satisfactory bank-angle tracking while the internal dynamics clearly exhibit input-to-state stable behavior. The nominal performance goal, which is achieved here, was to limit sideslip excursions to 1 deg in the case of a 10-deg step input in bank-angle command. This is a significant improvement as compared to the results obtained for the unmodified output (see Fig. 3). Figure 7 depicts the results for tracking of a segment of the Cycle 8 attitude command history. This simulation is conducted under aerodynamic model uncertainties. The nonlinear aerodynamic model utilized allows the perturbation of stability and control derivatives from their nominal values. Hence, differences in the actual and the inversion model dynamics arise. The impact of these perturbations will become obvious from the simulation plots. The simulation commences at an initial altitude of 62 km ($Ma = 20.0$) and terminates at 31 km altitude and a Mach number of $Ma = 4.3$. The breakdown of the pseudocontrol in the bottom row plots reveals that the neural-network adaptation is effective especially during the roll-reversal maneuvers. Despite the uncertainties, the internal dynamics remain bounded, which indicates that the robust pole placement serves its purpose. This in turn confirms that the assumption concerning the local exponential stability of the zero dynamics is indeed reasonable. In the top row plots the sideslip angle exhibits larger excursions during the first roll reversal. This is caused by the rapid large angle maneuver and especially the added effects of the model errors on the closed-loop system. However, because the sideslip angle is back in the vicinity of 1 deg within short time this is still regarded as acceptable. Guidance performance has not been found to be affected by this event. Further, the bank angle shows satisfactory tracking performance throughout the flight. Also depicted are the histories of the scheduled output parameters k_1, k_2, k_3. Recall that we have asserted that our formulation of the IID is sufficient for achieving satisfactory tracking performance. Obviously, this is corroborated by the simulation result. Finally, Figure 8 gives additional insight with regard to the approximation capability of the CMAC neural net. The model error Δ is compared to the output ν_{ad} of the neural net. For a more conspicuous illustration only a part of the whole simulation is shown. This part contains the first roll reversal that leads to large model error. In the ideal case the neural net would perfectly cancel the model error so that $\Delta + \nu_{ad} = 0$. In the longitudinal (right plot) as well as lateral (left plot) control channels, the neural net approximation is very close to the exact model error. This guarantees the good tracking performance seen in the preceding set of plots.

VIII. Conclusions

We have proposed an approach to attitude control of the X-38 reentry vehicle flying at high angles of attack. Specifically, dynamic inversion was applied as the underlying control method. Because only two actuators are available for control of the X-38, internal dynamics are inevitable. It has been shown how to stabilize the zero dynamics via output redefinition in conjunction with a robust pole placement. This in turn has allowed to apply a direct adaptive control law using neural networks. A theoretical justification for such a control law in the presence of internal dynamics has been given. Essentially, the control concept combines notions from nonlinear, robust, and neural adaptive control.

The proposed approach is equally applicable to other entry vehicle configurations. For most of the current and prospective configurations, rudder-type control effectors are rendered ineffective at high angles of attack. Furthermore, it is desirable to conserve thruster propellant by sparing the reaction control systems. This leaves only aileron and elevator-type aerosurfaces for control. Counteracting the resulting lack of controls by adding aerodynamic control surfaces to the airframe might alleviate the problem. However, this measure is likely to boost structural weight and the overall complexity of the system. Bearing this in mind, the proposed concept appears particularly compelling because, by exploiting the available minimal set of control effectors, it would eventually allow for a simpler and thus a less costly reentry system design.

Appendix: Numerical Design Examples

Some numerical examples for the developments in this paper are given. Two different flight conditions for controller design are considered. The system matrices A_{lat}, B_{lat}, C_{lat} are given for the lateral/directional motion when linearized about the equilibrium so that $\dot{x}_{\text{lat}} = A_{\text{lat}} x_{\text{lat}} + B_{\text{lat}} u_{\text{lat}}$. The controlled variable is $y_2 = C_{\text{lat}} x_{\text{lat}}$. The corresponding state and control are $x_{\text{lat}} = [\beta \;\; \mu \;\; \bar{p} \;\; \bar{r}]^T$ and $u_{\text{lat}} = \delta_a$, respectively.

$h = 40$ km, $\alpha = 36.44$ deg, $Ma = 7.06$

$$A_{\text{lat}} = \begin{bmatrix} -4.1399e^{-3} & 4.3212e^{-3} & 5.9391e^{-1} & -8.0453e^{-1} \\ 6.9023e^{-5} & -1.1260e^{-4} & 8.0453e^{-1} & 5.9391e^{-1} \\ -1.8299e^{+1} & 0 & 0 & 0 \\ 2.6969e^{+0} & 0 & 0 & 0 \end{bmatrix}$$

$$B_{\text{lat}} = \begin{bmatrix} 0 \\ 0 \\ 7.9872e^{+0} \\ -2.0942e^{-1} \end{bmatrix}$$

Zeros for $y_2 = \mu$ as controlled variable

$$-2.0968e^{-3} \pm 1.6764e^{+0}\, j$$

Output is redefined with parameters

$$k_1 = 2.5844e^{-1}, \qquad k_2 = -2.5057e^{+0}$$

$$k_3 = -1.3550e^{-1}, \qquad \kappa = 1$$

Zeros for redefined output with $C_{\text{lat}} = [2.5057e^{+0}\ \ 7.4145e^{-1}\ \ 8.2149e^{-1}\ \ 1.2410e^{+0}]$

$$-8.9938e^{-1}, \qquad -8.9981e^{-1} \pm 1.2306e^{+0}j$$

For this case the matrices P and Q as defined in the paper are

$$P = \begin{bmatrix} 0 & 0 & 1 \\ 0 & 0 & 7.7952e^{-1} \\ 0 & 0 & 0 \end{bmatrix}$$

$$Q = \begin{bmatrix} -1 & 0 & 0 \\ -7.7511e^{-1} & -4.1937e^{-3} & -2.6544e^{-1} \\ 0 & 1.0587e^{+1} & 0 \end{bmatrix}$$

$h = 70$ km, $\alpha = 40$ deg, $Ma = 24.41$

$$A_{\text{lat}} = \begin{bmatrix} 9.5412e^{-6} & 1.3184e^{-3} & 6.4279e^{-1} & -7.6604e^{-1} \\ -1.0762e^{-3} & -5.0287e^{-7} & 7.6604e^{-1} & 6.4279e^{-1} \\ -2.1733e^{+0} & 0 & 0 & 0 \\ 3.0566e^{-1} & 0 & 0 & 0 \end{bmatrix}$$

$$B_{\text{lat}} = \begin{bmatrix} 0 \\ 0 \\ 2.1573e^{+0} \\ -6.7575e^{-2} \end{bmatrix}$$

Zeros for $y_2 = \mu$ as controlled variable

$$4.8580e^{-4} \pm 5.6437e^{-1}j$$

Output is redefined with parameters

$$k_1 = -2.1004e^{+0}, \qquad k_2 = 1.1318e^{+0}$$

$$k_3 = -6.6050e^{-1}, \qquad \kappa = 1$$

Zeros for redefined output with $C_{\text{lat}} = [-1.1329e^{+0}\ \ 3.1004e^{+0}\ \ 1.0722e^{+0}\ \ 1.0417e^{+1}]$

$$-6.9749e^{-1}, \qquad -6.9512e^{-1} \pm 9.6802e^{-1}j$$

The matrices P and Q become

$$P = \begin{bmatrix} 0 & 0 & 1 \\ 0 & 0 & 8.9392e^{-1} \\ 0 & 0 & 0 \end{bmatrix}$$

$$Q = \begin{bmatrix} -1 & 0 & 0 \\ -8.9260e^{-1} & 9.7161e^{-4} & -9.0594e^{-2} \\ 0 & 3.5159e^{+0} & 0 \end{bmatrix}$$

Acknowledgments

This work was supported by the German Ministry of Education and Research and the State of Bavaria within the TETRA program under Contract 300-3245.2-1998.

References

[1]Isidori, A., *Nonlinear Control Systems*, Springer-Verlag, Berlin, 1989, Chap. 5.

[2]Enns, D., Bugajski, D., Hendrick, R., and Stein, G., "Dynamic Inversion: An Evolving Methodology for Flight Control Design," *International Journal of Control*, Vol. 59, No. 1, 1994, pp. 71–91.

[3]Reiner, J., Balas, G. J., and Garrard, W. L., "Flight Control Design Using Robust Dynamic Inversion and Time-Scale Separation," *Automatica*, Vol. 32, No. 11, 1996, pp. 1493–1504.

[4]Bharadwaj, S., Rao, A. V., and Mease, K. D., "Entry Trajectory Tracking Law via Feedback Linearization," *Journal of Guidance, Control, and Dynamics*, Vol. 21, No. 5, 1998, pp. 726–732.

[5]Snell, S. A., Enns, D. F., and Garrard, W. L., "Nonlinear Inversion Flight Control for a Supermaneuverable Aircraft," *Journal of Guidance, Control, and Dynamics*, Vol. 15, No. 4, 1992, pp. 976–984.

[6]Calise, A. J., and Rysdyk, R. T., "Nonlinear Adaptive Flight Control Using Neural Networks," *IEEE Control System Magazine*, Vol. 18, No. 6, 1998, pp. 14–25.

[7]Kim, S.-G., and Tahk, M.-J., "Output-Redefinition Based on Robust Zero Dynamics," AIAA Paper 98-4493, Aug. 1998.

[8]Gopalswamy, S., and Hedrick, J. K., "Tracking Nonlinear Non-Minimum Phase Systems Using Sliding Control," *International Journal of Control*, Vol. 57, No. 5, 1993, pp. 1141–1158.

[9]Gopalswamy, S., and Hedrick, J. K., "Control of a High Performance Aircraft with Unacceptable Zero Dynamics," *Proceedings of the American Control Conference*, Inst. of Electrical and Electronics Engineers Publications, Piscataway, NJ, 1992, pp. 1834–1838.

[10]Khalil, H. K., *Nonlinear Systems*, Prentice–Hall, Upper Saddle River, NJ, 1996, pp. 217–222, 552–554.

[11]Tigges, M. A., "Preliminary V-201 Entry Flight Profile with Landing Site Precision, Cycle-8," NASA V-201-NOI 175, Oct. 1998.

[12]Wallner, E., and Well, K. H., "Nonlinear Flight Control Design for the X-38 Using CMAC Neural Networks," AIAA Paper 2001-4042, Aug. 2001.

[13]Polycarpou, M. M., "Stable Adaptive Neural Control Scheme for Nonlinear Systems," *IEEE Transactions on Automatic Control*, Vol. 41, No. 3, 1996, pp. 447–451.

[14]Wallner, E., and Well, K. H., "Untersuchungen zur Nichtlinearen Flugregelung des Rückkehrfahrzeuges X-38," Inst. of Flight Mechanics and Control, Univ. of Stuttgart, TET-IFR-18-TR-5801, Stuttgart, Germany, Aug. 2002.

[15]Voegt, S., Burkhardt, J., Müller, S., Wallner, E., and Zimmermann, F., "CREDITS-Model and Algorithm Description," Astrium Space Infrastructure, TET-DASA-18-SW-2185, Bremen, Germany, Sept. 1999.